Micromechanical modeling of rate-dependent off-axis failure in thermoplastic composites

van der Meer, F.P.; Kovacevic, D.

Publication date
2022

Document Version
Final published version

Published in
Proceedings of the 20th European Conference on Composite Materials: Composites Meet Sustainability

Citation (APA)
van der Meer, F. P., & Kovacevic, D. (2022). Micromechanical modeling of rate-dependent off-axis failure in thermoplastic composites. In A. P. Vassilopoulos , & V. Michaud (Eds.), *Proceedings of the 20th European Conference on Composite Materials: Composites Meet Sustainability: Vol 4 – Modeling and Prediction* (pp. 589-596). EPFL Lausanne, Composite Construction Laboratory.

Composites Meet Sustainability – Proceedings of the 20th European Conference on Composite Materials,
ECCM20. 26-30 June, 2022, Lausanne, Switzerland

MICROMECHANICAL MODELING OF RATE-DEPENDENT OFF-AXIS FAILURE IN THERMOPLASTIC COMPOSITES

Dragan Kovačević [a,b], Frans P. van der Meer [c]

a: Delft University of Technology, P.O. Box 5048, 2600 GA Delft, The Netherlands
d.kovacevic-1@tudelft.nl
b: DPI, P.O. Box 902, 5600 AX Eindhoven, The Netherlands
c: Delft University of Technology, P.O. Box 5048, 2600 GA Delft, The Netherlands

Abstract: *A micromechanical finite deformation framework for modeling failure in unidirectional composites under rate-dependent off-axis loading is presented. The onset of global softening in the micromodel corresponds to macroscopic matrix crack formation. A thin slice representative volume element with periodic boundary conditions is used, which enables representation of three-dimensional stress states. A constant prescribed strain-rate is applied in the model with a dedicated arclength control method. Two failure mechanisms are included in the polymer matrix: visco-plasticity and microcracking. A cohesive surface methodology represents the microcracking process. Cohesive elements are added on the fly with a stress-based initiation criterion. For this purpose, a power law microcrack initiation criterion is proposed. The model is validated with experimental data from tensile tests on unidirectional carbon/PEEK composite material at prescribed strain-rate and different off-axis angles. The obtained maximum stress levels are used to generate Tsai-Hill failure envelopes for macroscopic transverse crack initiation.*

Keywords: thermoplastic composites; plasticity; microcracking; off-axis loading; strain-rate

1. Introduction

Modeling of failure processes in continuous fiber reinforced composite materials has drawn a lot of attention in the past decades. The customizable microstructure of composites offers more freedom to design the lightweight structures as compared to monolithic engineering materials such as steel and aluminum. Furthermore, the application of thermoplastic polymers as the composite matrix provides an opportunity for recycling of the deteriorated structural components. However, the heterogeneous structure of composites combined with the viscous nature of the polymer resin makes the prediction of the nonlinear material behavior under different loading scenarios more difficult. The majority of the theories proposed to study failure in composites do not explicitly account for the rate dependency of the process, but rather the strength parameters must be determined separately for every considered strain-rate. The micromechanical framework offers a good environment to readily accommodate rate dependent effects, providing that a suitable rate dependent material model is used for the matrix part. In this way the rate dependent failure of composites was studied by Govaert et al. [1], Bai et al. [2], Sato et al. [3], to name a few.

In this paper we propose a micromechanical model to study the rate dependent failure in unidirectional (UD) composites exposed to off-axis loading. The model is a Representative Volume Element (RVE), defined in local coordinate system aligned with carbon fibers. Being

  doi:10.5075/epfl-298799_978-2-9701614-0-0

defined in three-dimensional (3D) space, the RVE allows for the stress states in composites under general off-axis loading. The model undergoes finite deformations including two sources of nonlinearity in the matrix part. Visco-plasticity is included by the Eindhoven Glassy Polymer material model, whereas microcracking process is represented by a cohesive zone model. The onset of softening in the RVE response is taken as the point of failure and corresponds to the macroscopic crack formation. The model results are compared with experiments on unidirectional carbon/PEEK composite system subjected to a prescribed strain-rate under different off-axis angles.

2. Experiment

The experimental benchmark consists of UD C/PEEK laminates with different orientation of the reinforcement relative to the loading direction, tested at room temperature conditions until complete failure is observed [4], see Fig. 1. Because of the macroscopically uniform stress distribution in these tests, the test can be simulated with a single-scale microscopic model.

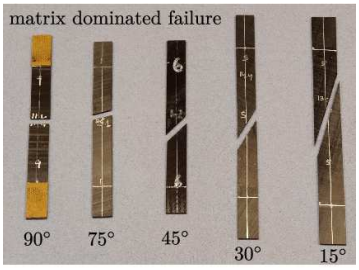

Figure 1. Fractured UD composite laminates under constant strain-rate, for different off-axis angles

The extensometer was used to measure the exact strain for the off-axis angle χ=90° at different strain-rates, and angles of: 75°, 45° and 30° at the strain rate of 10^{-4}/s. In all other cases, including χ=15° the extensometer was not utilized. In those cases, therefore, the compliance of the testing machine affects the results.

3. Micromechanical model

3.1 Problem definition

In order to develop the RVE model, first the homogenized deformation and stress state of the composite material exposed to a prescribed strain-rate is considered, see Fig. 2.

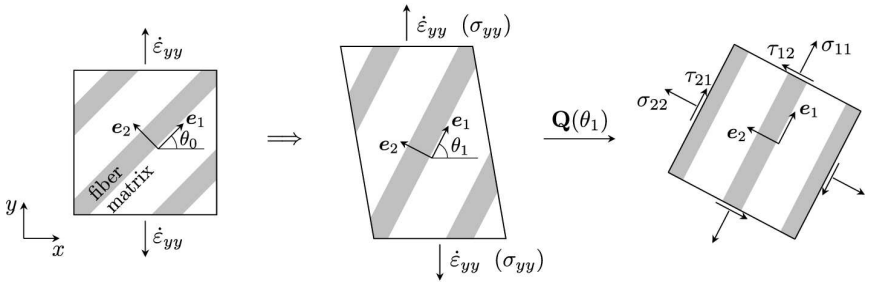

Figure 2. Strain-rate applied on UD composite material (left); deformation of the material due to applied strain-rate (middle); stress components in local coordinate system (right)

  doi:10.5075/epfl-298799_978-2-9701614-0-0

There is no restriction on the magnitude of strains in the material, implying that the local coordinate frame aligned with fibers may change orientation from the initial angle θ_0 to a new angle θ_1. Given this new angle, the transformation of the Cauchy stress to the local frame leads to the stress components acting on the material as shown in Fig. 2 (right).

Further analysis is done on the microlevel. The RVE with periodic boundary conditions is considered [5], such that one of its sides coincides with the reinforcement direction, see Fig. 3. The deformation and stress state of the RVE must be equivalent to that shown in Fig. 2. This means that the homogenized stresses on the RVE are equal to the corresponding components in Fig. 2 (right), and the deformation pattern of the RVE must correspond to the strain-rate applied in the global loading direction.

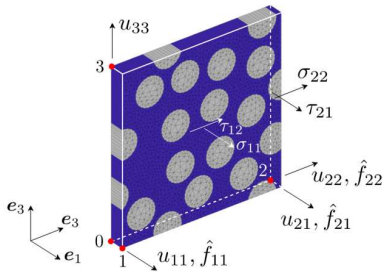

Figure 3. RVE with active displacements on master nodes and applied unit force components; master node displacements not indicated in the figure are set to zero; σ_{ij}, τ_{ij} required homogenized stress components on RVE

To satisfy these requirements a strain-rate based arclength model was formulated [6]. The constraint equation of the arclength model ensures that the RVE deforms according to the strain-rate imposed in global loading direction. In order to capture the finite strains in the material exactly, the unit force components of the arclength model are updated in every time step, accounting for the previous deformation and the change in orientation of the local frame from θ_0 to θ_1.

3.2 Material model for polymer matrix

Visco-plastic effects in the polymer matrix are included in the RVE by the Eindhoven Glassy Polymer (EGP) material model [7]. The EGP is an isotropic, elasto-viscoplastic material model that allows for the finite strains in the material. In the model, the stress is additively decomposed in three components: the hydrostatic stress, the hardening stress and the driving stress. The driving stress component introduces viscosity as well as plasticity in the model. It can also distinguish between different relaxation processes in the material, and for every relaxation process there might be multiple relaxation modes represented by different Maxwell elements connected in parallel. Material parameters used for the EGP model as described in [7] are listed in Table 1. The relaxation spectrum of one process, α, is considered and specified in Appendix.

Table 1: Material parameters for the EGP model

K [MPa]	G_r [MPa]	$\tau_{0\alpha}$ [MPa]	μ_α	$S_{\alpha\alpha}$	$r_{0\alpha}$	$r_{1\alpha}$	$r_{2\alpha}$
2600	14.2	1.386	.08	3	.95	1	-5

  doi:10.5075/epfl-298799_978-2-9701614-0-0

3.2 Material model for carbon fibers

It is assumed that carbon fibers do not undergo any failure process, therefore, the reinforcement responds elastically to the loading. A hyperelastic transversely isotropic material model [8] is selected to model this behavior, with a small modification as presented in [6]. The parameters of the material model are listed in Table 2. E_1 is the Young's modulus in the preferential stiffness direction, E_2 and v_{23} are the Young's modulus and Poisson's ratio in the plane of isotropy, G_{12} and v_{12} are the shear modulus and the Poisson's ratio defining behavior in the planes perpendicular to the isotropic plane. The modulus G_{12} has a value larger than usually reported [9], in order to achieve a good match in the initial slope between the experiment and the model.

Table 2: Material parameters for transversely isotropic material model

E_1 [GPa]	E_2 [GPa]	G_{12} [MPa]	v_{12}	v_{23}
125	15	45	.05	.3

3.3 Cohesive law for microcracking processes

Beside visco-plasticity, microcracking will also take place in the matrix part at higher stress levels. It is represented by means of a cohesive zone model that is governed by a mixed-mode damage cohesive law as explained by Liu et al. [10], and extended to 3D. Cohesive segments are added on the fly [11], when a stress-based initiation criterion is satisfied. At every time step the traction vector is computed on a potential cohesive surface, which may be any surface between two adjacent finite elements in the matrix part, or interface between carbon fibers and the matrix. The traction vector is decomposed in a component perpendicular to the fiber direction $t_\perp$ and a component parallel with the fibers $t_\parallel$. Then we propose an initiation criterion in the power law form:

$$\left(\frac{t_\perp}{f_\perp}\right)^m + \left(\frac{t_\parallel}{f_\parallel}\right)^n < 1 \tag{1}$$

where m and n are the power law coefficients, and $f_\perp$ and $f_\parallel$ are the strength parameters in the corresponding directions. In this study the following values are adopted: $m = 3$, $n = 2$, $f_\perp = 130$ MPa, $f_\parallel = 60$ MPa. For the fiber/matrix interface, the strength in direction parallel with the fibers is set higher, $f_\parallel = 75$ MPa.

The cohesive model also requires the fracture energy G_c as an input parameter. Observing the fractured specimens in Fig. 1, a conclusion arises that the mode of fracture changes for different off-axis angles. Hence, the value provided to the model interpolates between a value G_{cI} calibrated for χ=90° and a value G_{cII} calibrated for χ=15°, see Fig. 4. The G_c value provided to the model depends on the ratio between $t_\parallel$ and $t_\perp$ at the moment of initiation. For the problem at hand, this ratio provides a sufficient insight in the mode of fracture that will follow after the initiation takes place. This is because the load on the RVE increases almost proportionally, and there cannot be a huge variation in direction of the displacement jump. The value $\bar{t}_r$, after which the fracture energy cannot increase, represents the ratio between the initial homogenized shear stress τ_{21} and normal stress σ_{22} acting on the RVE for χ=15°, see Fig. 3.

  doi:10.5075/epfl-298799_978-2-9701614-0-0

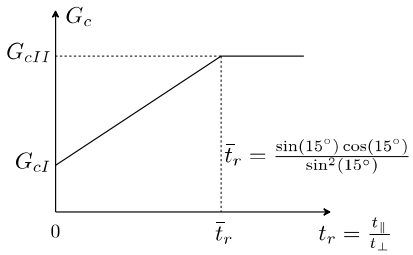

Figure 4. Fracture energy provided to cohesive law

The cohesive zone model also accounts for geometric nonlinear effect on the fracture process. This part is based on the work of Reinoso and Paggi [12], which is extended to 3D.

4. Results and discussion

In this section the simulation results are compared with the experiment. Homogenized stress-strain curves in the global loading direction are considered, see Fig. 2. The onset of softening in the RVE response is taken as the point of failure, and that point is compared with experimentally observed failure.

The strain-rate of 10^{-4}/s is applied on the RVE under several different off-axis angles. The obtained results are plotted in Fig. 5, together with the experimental stress-strain curves.

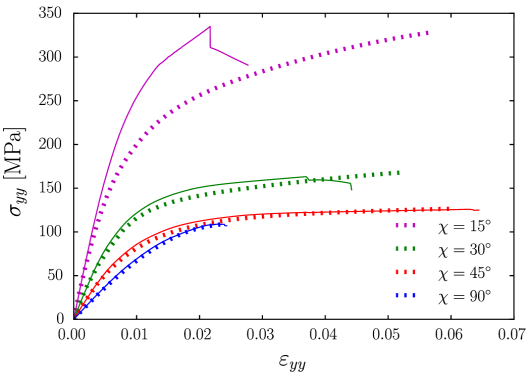

Figure 5. RVE response (solid) versus experiment (dotted) for strain rate 10^{-4}/s and different off-axis angles

For the off-axis angles in the range 30°-90° there is a good match with the experiments. For the off-axis angle χ=15°, there is an offset. One reason for this difference might be the fact that the extensometer was not used in this case. Also, the clamps of the testing machine introduce a restraining effect such that fibers close to the boundaries cannot freely rotate in an attempt to align with the loading direction. This is not the case with the RVE model, where the change in orientation of the RVE from the angle θ_0 to the angle θ_1 is allowed, see Fig. 2. This discrepancy in the kinematics implies a difference in the stress state. The difference gets more pronounced for lower off-axis angles, when a small variation in the angle makes a significant change in the stress taken by the fibers.

The fractured RVE for χ=30° is shown in Fig. 6. The contour plot indicates the distribution of the equivalent plastic strain in the model. The fracture plane is parallel with the reinforcement as is observed in the experiment, see Fig. 1. Also due to the higher strength of the interface in

  doi:10.5075/epfl-298799_978-2-9701614-0-0

direction parallel with the fibers, microcracking process is completely in the matrix. To support this fact, it is reported in the reference experiments that the interface mostly remains intact and the failure is indeed in the resin.

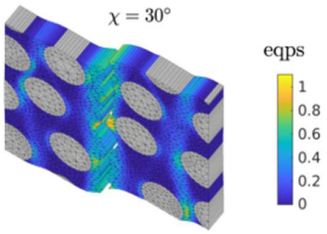

Figure 6. Example of fractured RVE with distribution of equivalent plastic *strain*

Now we make an attempt to construct a failure envelope based on the micromechanical simulations. The envelope intends to represent a stress at which the macroscopic crack forms for different off-axis angles. The Tsai-Hill failure criterion is considered [13]. Since the material is loaded in tension, this failure criterion gives reasonably accurate estimation of the material behavior. The idea presented in [14] is followed, such that the failure stress is a product of a reference failure stress $\sigma_{\text{ref}} = \sigma_{90^0}$ and a function depending on the off-axis angle $g(\chi)$. Coefficients needed to construct the function $g(\chi)$ are as follows: $R_{11} = \sigma_{0^0} / \sigma_{\text{ref}} = 18.94$, $R_{22} = R_{33} = \sigma_{90^0} / \sigma_{\text{ref}} = 1$, $R_{12} = 1.3$. The strength at χ=0°, $\sigma_{0^0} = 2063$ MPa was determined experimentally. The coefficient R_{12} is calibrated to achieve a good fit with the trend observed in the simulations. The Tsai-Hill failure criterion is compared with the failure stresses obtained from the RVE in Fig. 7.

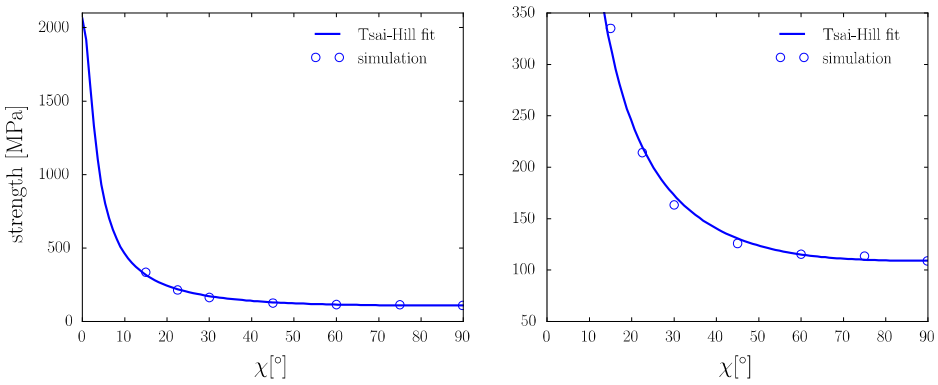

Figure 7. Tsai-Hill failure envelope versus simulation results; close-up view of the range covered by the RVE model (right)

Since no failure takes place in the carbon fibers, the model cannot accurately represent failure at low off-axis angles when the fibers bear most of the loading. Nevertheless, in the range that is covered by the present simulations a good fit is possible.

5. Conclusion

In this contribution a micromechanical framework to study rate-dependent failure in unidirectional composites under off-axis loading is introduced. The onset of softening in the micromodel represents macroscopic crack formation. The micromodel is a 3D RVE defined in the local coordinate frame aligned with the carbon fibers. This way, the stress states encountered

  doi:10.5075/epfl-298799_978-2-9701614-0-0

in off-axis loading scenarios can be reproduced in the RVE. A strain-rate is imposed on the RVE by means of a proper arclength model. The arclength model ensures that the homogenized kinematics of the RVE correspond with the strain-rate applied in the global loading direction. Finite deformations are allowed in the homogenized kinematics of the RVE as well as at every integration point, where appropriate constitutive models are used to represent the matrix part and the fibers. In the matrix part two different failure processes are included: visco-plasticity and microcracking. A cohesive zone model is utilized for the microcracking process in which geometric nonlinear effects are also included. The performance of the RVE model is compared with experiments on thermoplastic C/PEEK composite system at one prescribed strain-rate and different off-axis angles, at room temperature conditions. Based on the simulation results obtained, the Tsai-Hill failure fit is constructed. In the future work, failure of the model at different strain-rates will be considered and compared with experiments to validate the model.

6. Acknowledgement

This research forms part of the research programme of DPI, project #811t17.

The experimental work as part of the same project, performed at the University of Twente by Bharath Sundararajan and Leon Govaert is greatly acknowledged.

7. Appendix

Table 3: Relaxation spectrum of the EGP model

mode	$G_{\alpha,j}$ [MPa]	$\eta_{0\alpha,j}$ [MPa·s]	mode	$G_{\alpha,j}$ [MPa]	$\eta_{0\alpha,j}$ [MPa·s]
1	1045.52	$7.590 \cdot 10^{21}$	9	50.61	$9.198 \cdot 10^{10}$
2	400.03	$8.502 \cdot 10^{16}$	10	83.94	$2.272 \cdot 10^{10}$
3	46.06	$2.570 \cdot 10^{14}$	11	77.28	$8.756 \cdot 10^{8}$
4	87.28	$1.843 \cdot 10^{13}$	12	60.61	$2.874 \cdot 10^{7}$
5	72.43	$5.912 \cdot 10^{12}$	13	56.67	$1.127 \cdot 10^{6}$
6	63.03	$1.992 \cdot 10^{12}$	14	4.64	$3.851 \cdot 10^{4}$
7	45.46	$5.520 \cdot 10^{11}$	15	53.03	$1.840 \cdot 10^{3}$
8	42.43	$1.987 \cdot 10^{11}$	16	3.42	$4.961 \cdot 10^{1}$

8. References

1. Govaert LE, Schellens HJ, Thomassen HJM, Smit RJM, Terzoli L, Peijs T. A micromechanical approach to time-dependent failure in off-axis loaded polymer composites. Composites Part A 2001, 32:1697–1711.

2. Bai X, Bessa MA, Melro AR, Camanho PP, Guo L, Liu WK. High-fidelity micro-scale modeling of the thermo-visco-plastic behavior of carbon fiber polymer matrix composites. Composite Structures 2015, 134:132–141.

  doi:10.5075/epfl-298799_978-2-9701614-0-0

3. Sato M, Shirai S, Koyanagi J, Ishida Y, Kogo Y. Numerical simulation for strain rate and temperature dependence of transverse tensile failure of unidirectional carbon fiber-reinforced plastics. Journal of Composite Materials 2019, 53:4305–4312.

4. Sundararajan B, Govaert LE. Experimental part of the research programme of DPI, project #811t17, 2020.

5. Van der Meer FP. Micromechanical validation of a mesomodel for plasticity in composites. European Journal of Mechanics – A/Solids 2016, 60:58–69.

6. Kovačević D, Van der Meer FP. Strain-rate based arclength model for nonlinear microscale analysis of unidirectional composites under off-axis loading. Under review.

7. Van Breemen LCA, Klompen ETJ, Govaert LE, Meijer HEH. Extending the EGP constitutive model for polymer glasses to multiple relaxation times. Journal of the Mechanics and Physics of Solids 2011, 59:2191–2207.

8. Bonet J, Burton AJ. A simple orthotropic, transversely isotropic hyperelastic constitutive equation for large strain computations. Computer Methods in Applied Mechanics and Engineering 1998, 162:151–164.

9. Miyagawa H, Sato C, Mase T, Drown E, Drzal LT, Ikegami K. Transverse elastic modulus of carbon fibers measured by Raman spectroscopy. Materials Science and Engineering: A 2005, 412:88–92.

10. Liu Y, Van der Meer FP, Sluys LJ, Ke L. Modeling of dynamic mode I crack growth in glass fiber-reinforced polymer composites: Fracture energy and failure mechanism. Engineering Fracture Mechanics 2021, 243:107522.

11. Camacho GT, Ortiz M. Computational modelling of impact damage in brittle materials. International Journal of Solids and Structures 1996, 33:2899–2938.

12. Reinoso J, Paggi M. A consistent interface element formulation for geometrical and material nonlinearities. Computational Mechanics 2014, 54:1569–1581.

13. Azzi VD, Tsai SW. Anisotropic strength of composites. Experimental Mechanics 1965, 5:283–288.

14. Amiri-Rad A, Pastukhov LV, Govaert LE, Van Dommelen JAW. An anisotropic viscoelastic-viscoplastic model for short-fiber composites. Mechanics of Materials 2019, 137:103141.

  doi:10.5075/epfl-298799_978-2-9701614-0-0